High-Throughput Determination of Statistical Structure Information for Horizontal Carbon Nanotube Arrays by Optical Imaging

Shibin Deng, Jingyi Tang, Lixing Kang, Yue Hu, Fengrui Yao, Qiuchen Zhao, Shuchen Zhang, Kaihui Liu, and Jin Zhang**

The past few decades have witnessed the great progress in carbon nanotube research, which is now at the threshold of its real applications such as in nanoelectronics[1,2] and optoelectronics.[3] Just like mature semiconductor industry, in which structure and performance tests are prerequisite in all the processing steps, millions of nanotubes densely aligned on a wafer necessitate the characterization of their statistical structure information on growth substrates and in devices.[4] Up to now, many methods have been used to characterize the structure of nanotubes in different aspects and scales. Transmission electron microscopy[5] (TEM) and scanning tunneling microscopy[6] (STM) can provide atomic resolution images for nanotubes while the analytical area is quite limited (typically tens of nanometer). Scanning electron microscopy[7] (SEM) and atomic force microscopy[8] (AFM) are two most used methods to "count" the numbers of nanotubes, but they lack the ability of metallic/semiconducting (M/S) recognition and they even meet great challenges at lateral resolution as the density of nanotubes increases. Electrical measurement[9] and optical spectroscopic methods[10–13,17] are also adopted to determine the structure information but usually time-consuming. Generally, conventional methods are hard to provide statistical structure information with high-throughput which is necessary for development of carbon nanotubes now.

Optical imaging and spectroscopy were widely used to monitor the structure of massive bulk materials.[18] Notwithstanding its effectiveness, the implementation of optical imaging and spectroscopy in nanomaterials and nanodevices is still challenging mainly due to the small cross-section of light-matter interactions (considering the limited number of atoms in nanomaterials), especially for carbon nanotubes. To address this challenge, great efforts have been devoted to developing single-tube optical spectroscopy (e.g., Raman spectroscopy,[10] photoluminescence spectroscopy,[11] Rayleigh spectroscopy,[12,13] absorption spectroscopy,[14–16] and reflection spectroscopy[17]), through which one can now determine the structure information for individual nanotubes. However, single-tube optical spectroscopic methods are in nature of low throughput and therefore not suitable to determine the statistical structure information for millions of nanotubes efficiently. Compared with single-tube optical spectroscopic methods, optical imaging, which provides measurement ability in wide field, can drastically increase the throughput of optical measurement. Although the implantation of above-mentioned optical techniques to imaging is achievable, there are still hindrances for reliably measuring the statistical structure information from these techniques. Raman scattering only responds to the nanotubes in resonance with the laser. Photoluminescence lacks the ability to respond to metallic nanotubes. Rayleigh scattering and polarized light microscopy (absorption[15,16] or reflection[17]) are well suited to fast imaging, among which polarization-based reflective imaging can even achieve millisecond frame rate, showing its highest throughput. Nonetheless, recent works about these techniques only utilize the peak position of the spectroscopy to achieve qualitative measurement of individual nanotubes, quantitative using of the image information has not yet been reported.

Here we utilize optical imaging to achieve high-throughput measurement on structure information of massive nanotubes on substrates. The high-throughput ability is realized by direct use of the multicolor information in optical image with contrast enhanced over 10 folds. We successfully employ this technique to characterize carbon nanotube arrays on their line density and M/S ratio in a statistical way for submillimeter view field with integration time less than one second.

We utilize the convenient optical reflection imaging in this work (**Figure 1**a). For very thin atomic layered nanomaterials (horizontally aligned carbon nanotube array for example) on the transparent substrates, the optical reflection contrast ($\Delta R/R$) is directly related to the absorption in a linear way[19]

$$\frac{\Delta R}{R}=\frac{\left|E_{\mathrm{NT}}+E_{\mathrm{r}}\right|^{2}-\left|E_{\mathrm{r}}\right|^{2}}{\left|E_{\mathrm{r}}\right|^{2}}=\frac{2\left|E_{\mathrm{NT}}\right|}{\left|E_{\mathrm{r}}\right|}=\frac{4}{n_{\mathrm{s}}^{2}-1}A, \tag{1}$$

Dr. S. Deng, L. Kang, Dr. Y. Hu, Q. Zhao, S. Zhang, Prof. K. Liu, Prof. J. Zhang
Center for Nanochemistry
Beijing Science and Engineering Center for Nanocarbons
Key Laboratory for the Physics and Chemistry of Nanodevices
Beijing National Laboratory for Molecular Sciences
College of Chemistry and Molecular Engineering
Peking University
Beijing 100871, China
E-mail: khliu@pku.edu.cn; jinzhang@pku.edu.cn
J. Tang, F. Yao, Prof. K. Liu
State Key Laboratory for Mesoscopic Physics
School of Physics
Collaborative Innovation Center of Quantum Matter
Peking University
Beijing 100871, China

DOI: 10.1002/adma.201505253

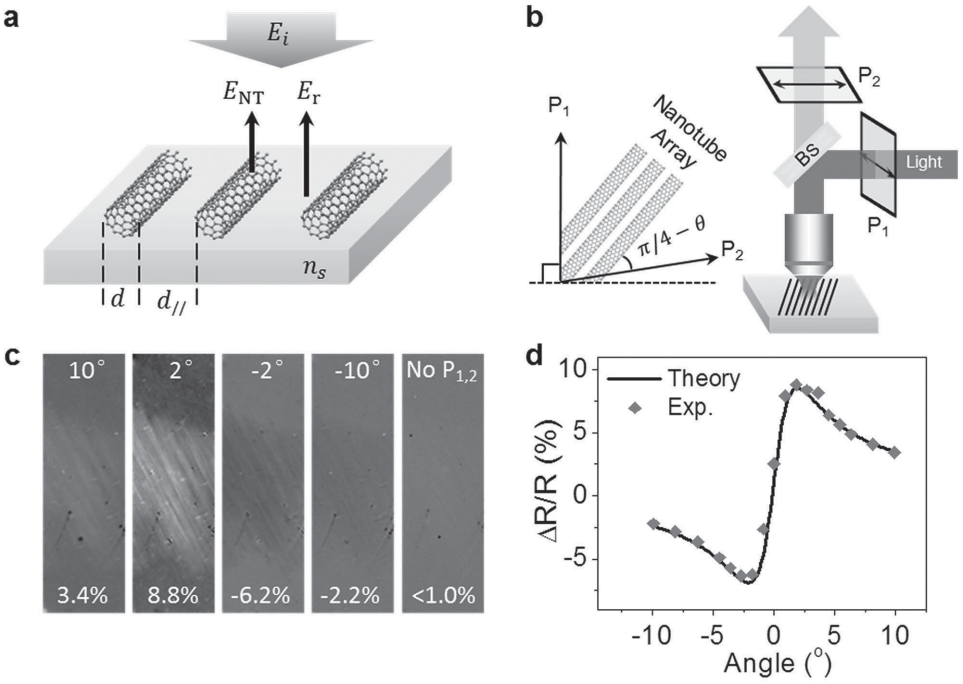

Figure 1. Optical image of carbon nanotube arrays with enhanced optical contrast. a) Schematic concept of reflection optical contrast for carbon nanotube arrays. b) Schematic configuration of polarization microscopy with carbon nanotube arrays. The incoming and outgoing polarizers are nearly vertically placed with θ deviation and carbon nanotube array axis is set 45° to the incoming polarizer. c) Typical optical images of nanotube array at different θ. The bright-to-dark transition of nanotube images between $\theta = \pm 2°$ is caused by sign change of referenced refection electrical field associated with θ. d) The dependence of optical contrast on θ for the nanotube array in (c). The black curve is the theoretical fitting considering the polarization impurity effect in our optical setup.

where E_{NT} and E_r are the nanotube-scattered electric field and substrate-reflected electric field at the detector, respectively; n_s is the refractive index of the substrate; A is the nanotube optical absorption; $(E_{NT}/E_r)^2$ term is orders of magnitude smaller than (E_{NT}/E_r) term and therefore neglected.

Since optical absorption is the most fundamental optical parameter characterizing the light-matter interactions in materials, in principle, one can use the optical reflection image to determine various kinds of structure information for any material. However, the direct acquisition of optical image for nanotube arrays on substrates is conventionally believed to be challenging due to its very small optical signal (down to $10^{-3} - 10^{-4}$). Here we utilize the depolarization effect in anisotropic 1D materials to drastically enhance the optical contrast of carbon nanotube arrays by manipulating the polarization, which has been proved to be very effective on individual carbon nanotubes.[15–17] Basically, two nearly vertically crossed polarizers (with deviation angle to 90°) are respectively placed in the incoming (P_1) and outgoing (P_2) light path ways and the nanotubes are oriented at 45° with respect to P_1 (Figure 1b). Under this configuration, the E_{NT} term is mainly maintained ($E_{NT}^{//} \approx E_{NT}/\sqrt{2}$) while the E_r term is greatly suppressed ($E_r^{//} = E_r \sin\theta$) and therefore the optical contrast can be greatly enhanced (by $\approx 1/(\sqrt{2}\sin\theta)$). This concept can be directly verified by reviewing the optical images taken at different θ angles (Figure 1c). It is obvious that without polarization manipulation, one can barely see any signal from nanotubes (optical contrast less than 1.0%); with $|\theta|$ decreasing to 2°, the nanotube array images get obviously clear with contrasted >6% (the bright-to-dark transition of nanotube images between $\theta = \pm 2°$ is caused by sign change of $E_r^{//}$ associated with θ). With further detailed analysis of the optical contrast considering the unavoidable polarization impurities in the optical setup, we find that

$$\frac{\Delta R}{R} = \frac{4}{n_s^2 - 1} A f(\theta, e), \tag{2}$$

where $f(\theta, e)$ is the factor induced by polarization manipulation (see details in Section S1 in the Supporting Information). Using Equation (2), we can nicely describe the θ-dependent optical contrast (Figure 1d), which give out the reliable optical absorption A of carbon nanotube arrays.

Once we get the absorption information of nanotube arrays from the optical image contrast, we can obtain their various kinds of statistical structure information. The most two important pieces of information for the coming electronic and optoelectronic applications in nanotube arrays are line density and M/S nanotube ratio. The industry has actually established a clear standard for nanotube growth community:[2] Before 2020, line density should be larger than 125 tubes μm^{-1} and M/S ratio should be smaller than 0.0001%. To reach such standard, one needs not only to optimize the growth conditions but also to characterize the as-grown samples for reliable and prompt feedback. Below, we will demonstrate how we can use our optical imaging method to determine the line density and M/S ratio in the nanotube arrays.

We first determine the line density of nanotube arrays from their integral optical contrast in the optical image. According to the approximation sum rule, the integrated absorption per atom in a wide spectral range is nearly the same for all graphitic materials. Therefore, we can directly get the total carbon atom numbers from the integral absorption. Then the nanotube array line density can be obtained by

$$l = \frac{A}{\left(\pi \bar{d}\, s_0 \sigma\right)} \tag{3}$$

where l, A, $\bar{d}$, s_0, σ are the nanotube line density, absorption, mean diameter, areal in-plane atom density, and the absorption cross-section per atom, respectively (see details in Section S2 in the Supporting Information). Since s_0 is of constant value, σ has been systematically given out by the previous work,[15] and the mean diameter $\bar{d}$ in our nanotube array samples is known to be ≈1.4 nm (Section S3 in the Supporting Information), we can get l directly from the optical absorption A. The two samples with optical images shown in **Figure 2**a,d have line density of 20 and 50 tubes μm^{-1}, respectively.

Conventionally, scanning electron microscopic (SEM) or atomic force microscopic (AFM) image is mostly used to determine the line density of nanotube arrays. However, these two techniques have the limitation in the characterization of samples with high density. Due to the discharge effect in SEM or the tip convolution effect in AFM, the obtained lateral diameter will be inevitably broadened and the adjacent nanotubes will become indistinguishable when the line density exceeds certain threshold. In our experiment, the maximum line density that can be reliably determined are ≈10 tubes μm^{-1} for SEM and ≈30 tubes μm^{-1} for AFM. For examples, as for lower density of 20 tubes μm^{-1}, our optical image method (Figure 2a) and AFM (Figure 2b) can both work well and give out consistent result (SEM in Figure 2c fails to give out the right value); as for relatively higher density of 50 tubes μm^{-1}, our optical image method (Figure 2d) still work but either AFM (Figure 2e) or SEM (Section S4, Supporting Information) fails to give out the right value. The limitation in our optical imaging method comes from the "thin film" assumption, and even for the case that nanotubes are tightly packed (corresponding to line density of $1/(\bar{d} + 0.34\ \text{nm}) \approx 600$ tubes μm^{-1}; 0.34 nm comes from the van der Waals intertube distance limitation), the assumption is still right and our method can determine the line density unambiguously. Admittedly, the analytical power of AFM and SEM can still be enhanced by carefully choosing the equipment and experimental condition,[20] but obviously, to characterize the line density up to 125 tubes μm^{-1} as required by the industry, conventional techniques become very difficult if possible and our method still works well.

We further determine the M/S ratio of nanotube arrays from their color-resolved optical contrast in the optical image. From the nanotube quantization analysis, nanotube optical transitions are quantized into $k = 2p/3d$, where k is the momentum in the graphene brillouin zone, d is the nanotube diameter and p is an integer. For metallic nanotubes, p = 3, 6 for M_{11} and M_{22} optical transitions; for semiconducting nanotubes, p = 1, 2, 4, 5 for S_{11}, S_{22}, S_{33}, and S_{44} optical transitions. Therefore, for nanotubes with similar diameter, their optical transition peak positions or colors are different for M and S nanotubes.

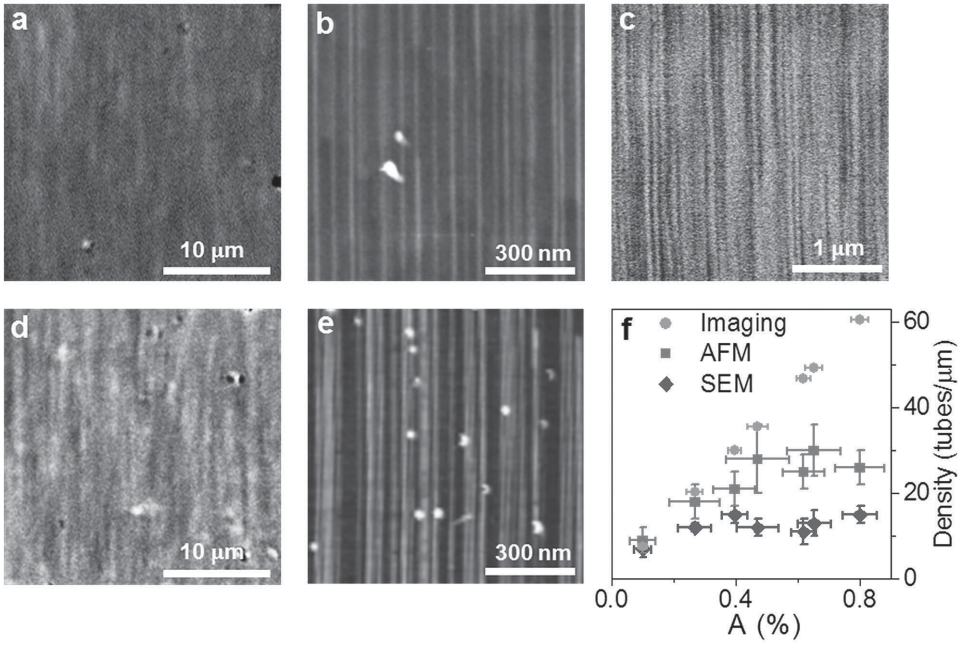

Figure 2. Determination of the line density for carbon nanotube arrays by integral optical contrast. a) The optical image of carbon nanotube array on sapphire with line density of ≈20 tubes μm^{-1}. b,c) The typical AFM and SEM images corresponding to (a). The AFM gives out consistent line density as from optical imaging but SEM fails to characterize. d) The optical image of carbon nanotube array on sapphire with line density of ≈50 tubes μm^{-1}. e) The typical AFM image corresponding to (d). The line density is already too high to determine for AFM method. f) The comparison between SEM, AFM, and optical imaging method in determining the line density. SEM and AFM methods become invalid for line density exceeding ≈10 and ≈30 tubes μm^{-1}, respectively.

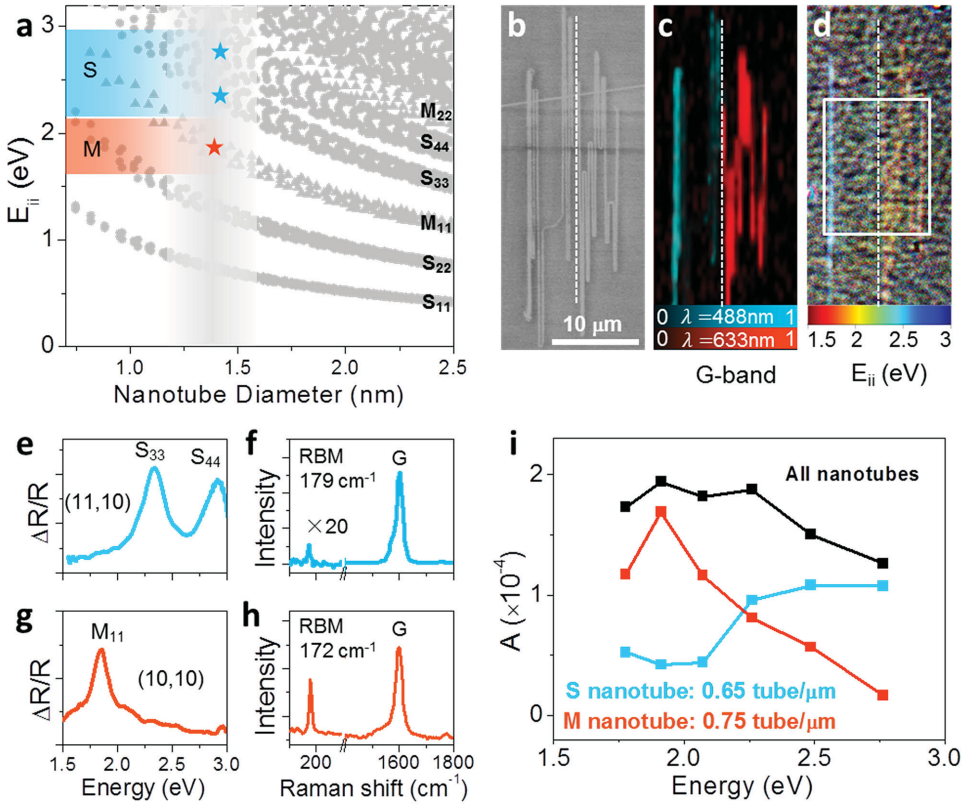

Figure 3. Determination of the M/S ratio for carbon nanotube array by color-resolved optical contrast. a) The Kataura plot generated from the experimental atlas of nanotube optical transitions.[13] The vertical gray bar shows the diameter region of our as-grown nanotube arrays. b–d) SEM, Raman G-mode mapping, and optical image of a "U" hetero-nanotube array on quartz. The vertical dashed lines indicate the boundary positions for the two types of nanotubes. e,f) Reflection optical spectrum and Raman spectrum for the left part nanotube in (b–d). It is a semiconducting (11, 10) nanotube. g,h) Reflection optical spectrum and Raman spectrum for the right part nanotube in (b–d). It is a metallic (10, 10) nanotube. i) Color-resolved optical contrast for the whole box region in (d) and its decomposition into S and M nanotube contribution. The M/S ratio is determined to be around 1.1 by either the integrated optical contrast from the separated S and M nanotube regions or the color-resolved optical contrast for the whole S and M nanotube regions.

This conclusion can be seen from the Kataura plot (**Figure 3**a), which shows the relation between the optical transition energy E_{ii} and the nanotube diameter (this plot is generated from the atlas of nanotube optical transitions[13]). For example of our as-grown nanotube with diameter around 1.4 nm, the M tubes have M_{11} optical transitions at 1.8–2.2 eV while S tubes have S_{22} and S_{33} optical transitions at 2.2–3.0 eV in the visible-violet range. Therefore, in principle we can determine the M/S ratio by evaluating the optical contrast ratio between different color regions.

To clearly verify the validity in determining the M/S ratio of nanotube arrays by color-resolved optical contrast, we choose a special "U" shape hetero-nanotube sample (Figure 3b). The reflection (Figure 3e,g) and Raman spectroscopy (Figure 3f,h) show that the left part is of S type (11, 10) and the right part is of M type (10, 10). From Raman G mode mapping (Figure 3c), we can find the boundary between the two types (as indicated by vertical dashed line). Using the integral optical contrast of the two regions as separated by the dashed line and outlined by the white box in Figure 3d, we obtain the line density of 0.71 tubes μm^{-1} for left S nanotube and 0.77 tubes μm^{-1} for right M nanotube and the M/S ratio is 1.08. Alternatively, we can directly use the color-resolved optical contrast (Figure 3i) without distinction about the S and M regions to determine the M/S ratio (see details in Section S5 in the Supporting Information). The ratio is obtained as 1.15, close to the above value of 1.08. The discrepancy should be from the background inhomogeneity of this tested sample. Here for this special "U" shape hetero sample, both the integral and color-resolved optical image methods can determine the M/S ratio. In more general cases, we cannot resolve the M and S nanotube region but the color-resolved optical image method will still work. We further use this method to determine the M/S ratio in a high density nanotube arrays (50 tubes μm^{-1}) and obtain the value of 0.57 (Section S5, Supporting Information). For randomly distributed chirality, the theoretical value of M/S ratio is 0.50. Which means that, without special growth control, the nanotube type is mostly random. There have been several optical techniques[12,13,15–17] which also use the transition energy difference to distinguish M/S tubes on substrate, however, only when the density is lower than ≈1 tubes μm^{-1}. This shortcoming is a direct result of diffraction limit. As discussed above, our technique does not take resolving tubes as a premise, and it can work well even when the nanotubes are tightly packed as a continuous film. Recently great efforts have been put on growing high density S-rich nanotube arrays but the current purity is still not high enough to reach 99.9999% standard. Our

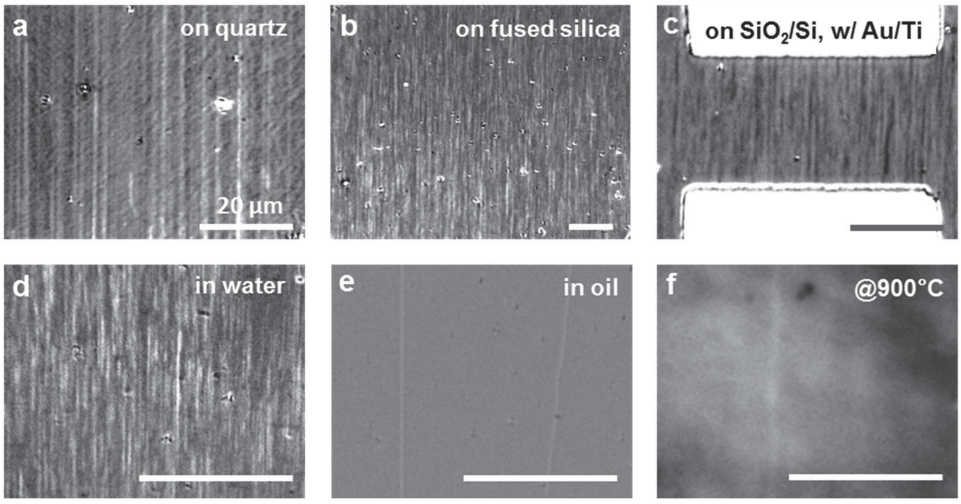

Figure 4. Optical images of carbon nanotube on various substrates and in diverse environments. Optical images of carbon nanotubes on a) fused silica, b) quartz, c) SiO_2/Si substrates with electrodes, d) in water, e) in oil, and f) under 900 °C in argon gas.

method can simultaneously provide the fast feedback about both density and S richness and should definitely accelerate the realizing the goal of very pure and high density S nanotubes. Our technique is based on optical imaging (with contrast enhanced by polarization manipulation), and therefore quite versatile for different substrates and environments. Actually, we can get nanotube images on different substrates of sapphire (Figure 2), quartz (**Figure 4**a), fused silica (Figure 4b), and SiO_2/Si with electrodes (Figure 4c); immersed in different liquids of water (Figure 4d) and oil (Figure 4e); and even under high temperature of 900 °C (Figure 4f). The versatility of our technique indicates its wide potential applications, such as feeding back to the growth, monitoring the device performance, sensing the biosystem and in situ studying nanotube growth. Finally, we would like to add a note for our method. It can determine statistical information quite well for nanotube arrays due to their relatively narrow diameter distribution, thanks to the great progresses in the controllable growth in the nanotube community. For general nanomaterial characterization, we should review the structure distribution of individuals before applying our method for massive characterization. Fortunately, in most nanomaterials growth, scientists can well control the materials into a very narrow structure distribution and our method will work.

In summary, we developed an optical imaging method to determine the statistical structure information of massive carbon nanotubes with submillimeter view field and subsecond characterization time. We vision that our method will accelerate the controllable growth of carbon nanotubes with high density and high semiconducting purity and eventually promote the industrial nanotube applications. Our method should also find its application in fast characterizing broad range of nanomaterials and in situ monitoring the nanoscale electronic and biological devices.

Experimental Section

Synthesis and Conventional Characterization of Single-Walled Carbon Nanotube Arrays on Different Substrates: Carbon nanotubes were grown in chemical vapor deposition (CVD) system. In particular, ST-cut quartz, a-plane sapphire, and 90 nm SiO_2/Si wafer (Hefei Kejing Materials Technology Company, China) were used as substrates. $Fe(OH)_3$/ethanol solution, as catalyst precursor, was dispersed onto the substrates. The CVD system was purged with argon, a flow of hydrogen and argon (through an ethanol bubbler) was introduced for the growth of SWNTs at the desired temperature. The morphology, diameters, and chiral indices of as-grown SWNTs were inspected with scanning electron microscopy (Hitachi S4800 field emission, Japan), atomic force microscopy (NanoScope IIIA, Veeco Co.), Raman spectroscopy (Horiba HR800) and home-built single-tube high-contrast reflection spectroscopy.[17] The home-built single-tube high-contrast reflection spectroscopy employs a supercontinuum laser as light source and a spectrometer as photon energy analyzer, it can measure the contrast spectroscopy of carbon nanotubes in small spot area (typically 1×1 μm^2).

Optical *Reflection Image Measurements*: As shown in Figure 1b, an optical microscope (Olympus BX51) equipped with a 50× objective (N.A.=0.75, air), a 60× objective (N.A.=1.25, water), a 100× objective (N.A.=1.25, oil), a 50× objective (N.A.=0.5, long working distance for imaging high temperature sample), two polarizers (Daheng optics, GCL-050003) and two cameras were used to capture the polarized optical images. For Figure 3d, a monochrome camera (Andor Zyla 4.2) and a series of band-pass filters with 50 nm bandwidth (Edmund Optics) were used; for all other images, a color camera (Olympus DP71) was used. A tungsten–halogen lamp was used as the light source, the reflective mode was used, one polarizer was located in the incident beam with its transmission axis set horizontally, and the second polarizer was placed in the reflective beam with its transmission axis set to a small angle θ from the vertical direction.

A Kohler illuminator provides evenly dispersed light across the plane of field of view. The aperture iris diaphragm and the field iris diaphragm enable convenient controls of incident beam. For a balance of light intensity and polarization purity, the aperture iris diaphragm was set to an effective N.A. of ≈0.3, the polarization extinction for the reflected light was then maintained above 10^3 for R, G, B channels. The corresponding reflection optical contrast was enhanced by about 15 folds. The field iris diaphragm was used to eliminate excess light. For birefringence substrates, refractive index matching was performed to suppress the depolarized light from the back surface. Bare substrate plates were used as reference. The typical image exposure time is 0.5 s.

As from its definition, the optical contrast was obtain by

$$\frac{\Delta R}{R} = \frac{R_{CNT+S} - R_S}{R_S}$$

in which R_{CNT+S} and R_S are the reflection for the CNT on substrate and reflection for bare substrate, respectively. (A small area on the substrate was purposely made without nanotube growth for generating the R_S). Technically, R_{CNT+S} and R_S was measured by averaging the image brightness of every single pixel for the regions of interest (ROI). And then the integral optical contrast by

$$\text{integral optical contrast} = \frac{\sum \frac{\Delta R}{R} \cdot E_i}{\sum E_i}$$

in which E_i is the bandwidth (in energy) for the specific filter used in imaging. Experimentally, the integral optical contrast was calculated by averaging the optical response in wide spectral range, for example, R, G, B channels from a color CCD.

Acknowledgements

S.D. and J.T. contributed equally to this work. The authors are grateful to Jinying Wang and Zhirong Liu (Peking University, China) for their helpful discussions. The authors also thank Liming Xie (National Center for Nanoscience and Nanotechnology, China) for the help with imaging in water. This work was supported by Beijing Municipal Science and Technology Commission (D141100000614001), NSFC (21233001, 21129001, 51272006, 51432002, 51121091, 51522201, 11474006, and 91433102), MOST (2011CB932601) and the National Program for Thousand Young Talents of China.

Received: October 25, 2015
Revised: November 30, 2015
Published online: January 14, 2016

[1] a) P. Avouris, Z. Chen, V. Perebeinos, *Nat. Nanotechnol.* **2007**, *2*, 605; b) M. M. Shulaker, G. Hills, N. Patil, H. Wei, H.-Y. Chen, H. S. PhilipWong, S. Mitra, *Nature* **2013**, *501*, 526.
[2] A. D. Franklin, *Nature* **2013**, *498*, 443.
[3] a) J. Chen, V. Perebeinos, M. Freitag, J. Tsang, Q. Fu, J. Liu, P. Avouris, *Science* **2005**, *310*, 1171; b) P. Avouris, M. Freitag, V. Perebeinos, *Nat. Photonics* **2008**, *2*, 341; c) N. M. Gabor, Z. Zhong, K. Bosnick, J. Park, P. L. McEuen, *Science* **2009**, *325*, 1367; d) X. Dang, H. Yi, M.-H. Ham, J. Qi, D. S. Yun, R. Ladewski, M. S. Strano, P. T. Hammond, A. M. Belcher, *Nat. Nanotechnol.* **2011**, *6*, 377.
[4] a) S. Maruyama, R. Kojima, Y. Miyauchi, S. Chiashi, M. Kohno, *Chem. Phys. Lett.* **2002**, *360*, 229; b) K. Hata, D. N. Futaba, K. Mizuno, T. Namai, M. Yumura, S. Iijima, *Science* **2004**, *306*, 1362.
[5] S. Iijima, T. Ichihashi, *Nature* **1993**, *363*, 603.
[6] a) T. W. Odom, J. L. Huang, P. Kim, C. M. Lieber, *Nature* **1998**, *391*, 62; b) J. W. G. Wildoer, L. C. Venema, A. G. Rinzler, R. E. Smalley, C. Dekker, *Nature* **1998**, *391*, 59.
[7] K. Ryu, A. Badmaev, C. Wang, A. Lin, N. Patil, L. Gomez, A. Kumar, S. Mitra, H. S. P. Wong, C. Zhou, *Nano Lett.* **2009**, *9*, 189.
[8] a) L. Ding, D. Yuan, J. Liu, *J. Am. Chem. Soc.* **2008**, *130*, 5428; b) Y. Hu, L. Kang, Q. Zhao, H. Zhong, S. Zhang, L. Yang, Z. Wang, J. Lin, Q. Li, Z. Zhang, L. Peng, Z. Liu, J. Zhang, *Nat. Commun.* **2015**, *6*, 6099.
[9] A. Javey, J. Guo, Q. Wang, M. Lundstrom, H. J. Dai, *Nature* **2003**, *424*, 654.
[10] a) A. Jorio, R. Saito, J. H. Hafner, C. M. Lieber, M. Hunter, T. McClure, G. Dresselhaus, M. S. Dresselhaus, *Phys. Rev. Lett.* **2001**, *86*, 1118; b) C. Fantini, A. Jorio, M. Souza, M. S. Strano, M. S. Dresselhaus, M. A. Pimenta, *Phys. Rev. Lett.* **2004**, *93*, 147406; c) H. Telg, J. Maultzsch, S. Reich, F. Hennrich, C. Thomsen, *Phys. Rev. Lett.* **2004**, *93*, 177401.
[11] a) S. M. Bachilo, M. S. Strano, C. Kittrell, R. H. Hauge, R. E. Smalley, R. B. Weisman, *Science* **2002**, *298*, 2361; b) J. Lefebvre, J. M. Fraser, P. Finnie, Y. Homma, *Phys. Rev. B* **2004**, *69*, 075403.
[12] a) M. Y. Sfeir, F. Wang, L. M. Huang, C. C. Chuang, J. Hone, S. P. O'Brien, T. F. Heinz, L. E. Brus, *Science* **2004**, *306*, 1540; b) D. Y. Joh, J. Kinder, L. H. Herman, S. Y. Ju, M. A. Segal, J. N. Johnson, G. K. L. Chan, J. Park, *Nat. Nanotechnol.* **2011**, *6*, 51; c) W. Wu, J. Yue, X. Lin, D. Li, F. Zhu, X. Yin, J. Zhu, J. Wang, J. Zhang, Y. Chen, X. Wang, T. Li, Y. He, X. Dai, P. Liu, Y. Wei, J. Wang, W. Zhang, Y. Huang, L. Fan, L. Zhang, Q. Li, S. Fan, K. Jiang, *Nano Res.* **2015**, *8*, 2721.
[13] K. H. Liu, J. Deslippe, F. J. Xiao, R. B. Capaz, X. P. Hong, S. Aloni, A. Zettl, W. L. Wang, X. D. Bai, S. G. Louie, E. G. Wang, F. Wang, *Nat. Nanotechnol.* **2012**, *7*, 325.
[14] S. Berciaud, L. Cognet, P. Poulin, R. B. Weisman, B. Lounis, *Nano Lett.* **2007**, *7*, 1203.
[15] K. H. Liu, X. P. Hong, S. Choi, C. H. Jin, R. B. Capaz, J. Kim, W. L. Wang, X. D. Bai, S. G. Louie, E. G. Wang, F. Wang, *Proc. Natl. Acad. Sci. USA* **2014**, *111*, 7564.
[16] J. Lefebvre, P. Finnie, *Nano Res.* **2011**, *4*, 788.
[17] K. H. Liu, X. P. Hong, Q. Zhou, C. H. Jin, J. H. Li, W. W. Zhou, J. Liu, E. G. Wang, A. Zettl, F. Wang, *Nat. Nanotechnol.* **2013**, *8*, 917.
[18] F. D. Bloss, *An Introduction to the Methods of Optical Crystallography* Holt, Rinehart and Winston, New York **1961**.
[19] a) K. F. Mak, M. Y. Sfeir, Y. Wu, C. H. Lui, J. A. Misewich, T. F. Heinz, *Phys. Rev. Lett.* **2008**, *101*, 196405; b) F. Wang, Y. Zhang, C. Tian, C. Girit, A. Zettl, M. Crommie, Y. R. Shen, *Science* **2008**, *320*, 206.
[20] a) D. G. de Oteyza, P. Gorman, Y.-C. Chen, S. Wickenburg, A. Riss, D. J. Mowbray, G. Etkin, Z. Pedramrazi, H.-Z. Tsai, A. Rubio, M. F. Crommie, F. R. Fischer, *Science* **2013**, *340*, 1434; b) J. Zhang, P. Chen, B. Yuan, W. Ji, Z. Cheng, X. Qiu, *Science* **2013**, *342*, 611.